ANNALS OF GEOPHYSICS, 68, 3, NS330, 2025; doi:10.4401/ag-9150
OPEN ACCESS

The use of the inversion of single-station Rayleigh wave ellipticity curve in routine site investigation: numerical inversion and case-studies

Ana Carolina Antunes[1], Paula Teves-Costa[2], Rui Carrilho Gomes[*,1]

(1) CERIS, Instituto Superior Técnico, Universidade de Lisboa, Lisboa, Portugal
(2) Universidade de Lisboa, Faculdade de Ciências, Instituto Dom Luiz, Lisboa, Portugal; European Centre on Urban Risks (CERU), Lisboa, Portugal

Article history: received September 5, 2024; accepted May 14, 2025

Abstract

Non-invasive single-station ambient vibration recordings have become very common nowadays for microzonation studies. Usually, these records are processed using Nakamura's method to determine the horizontal-to-vertical spectral ratio (H/V) curve, but the Rayleigh waves' ellipticity curve can also be determined and inverted alone or combined with data acquired using other surface wave methods. Since single-station ambient vibration-based analyses are a very cost-effective technique, this paper studies the reliability of the shallow ground structure that results from the ellipticity curve inversion, with prior knowledge on the ground profile characteristics, as is common in urban areas. The inversion of the ellipticity curve of a large set of shear wave velocity profiles (V_s-profiles) was simulated numerically to characterize the uncertainty. Three normally dispersive case studies in Lisbon County were used to evaluate the technique. RayDec was used to obtain experimental ellipticity curves inverting the right flank and the complete curve. It is shown that the Rayleigh wave ellipticity curve inversion can be a valuable and cost-effective preliminary site investigation technique, adopting a constrained inversion (based on some prior knowledge), to support the preliminary design stage of geotechnical works.

Keywords: Non-invasive Seismic Methods; Ellipticity Curve; Rayleigh Waves; Shear Wave Velocity Profile; Shallow Structure

1. Introduction

In the last decade, seismic methods based on ambient vibration recordings to characterise the soil structure and seismic microzonation studies increased popularity (e.g., Leyton et al., 2013; Pastén et al., 2016; Yilar et al., 2017; Molnar et al., 2020; Oliveira et al., 2020). Multi-station (array) or single-station recordings are often used to characterise the shear wave velocity of the shallower layers (Fäh et al., 2003; Poggi et al., 2012; Corchete, 2013; Hobiger et al., 2013; Hakim et al., 2019; Di Giulio et al., 2020; Issaadi et al., 2020; Maklad et al., 2020), but their

uncertainty is dependent on the technique used and on the previous information available on the site stratification to constrain the inversion procedure.

Single-station measurements are usually used to compute the horizontal-to-vertical spatial ratio (H/V) curve, by applying the Nakamura method (Nakamura, 1989) for microzonation purposes. Lunedei and Malischewsky (2015) reviewed the ambient vibrations based analysis technique theory.

H/V curve contains the contribution of all seismic waves, while the ellipticity curve depends only on the Rayleigh waves, the wave field.

The relative proportion of different wave type depends on site conditions, and especially on the impedance contrast. For the one-dimensional layered structure, the H/V peak frequency always provides a good estimate of the fundamental resonance frequency regardless of the H/V peak origin, such as Rayleigh wave ellipticity, Airy phase of Love waves, or S-wave resonance (Bonnefoy-Claudet et al., 2008).

The Rayleigh-waves can be extracted from the ambient vibration wavefield by processing techniques (e.g., Hobiger et al., 2009) to build the ellipticity curve, that corresponds to ratio between the horizontal and vertical components of the elliptical motion described by Rayleigh waves, as a function of frequency.

The inversion of the ellipticity curves can provide information on the properties of the shallow layers (e.g., Hobiger et al., 2013; Maranò et al., 2017), but its interest for practical application still needs to be exploited.

The inversion assumes a one-dimensional horizontally layered medium and the fundamental mode of vibration. The experimental ellipticity curve may be influenced by higher modes, typically above the trough, and its inversion as corresponding to the fundamental mode can lead to biased results.

The inversion of the Rayleigh wave ellipticity curve can also be performed jointly with the dispersion curve obtained by array surface wave methods (e.g., Gouveia et al., 2016). Poggi et al. (2012) used Rayleigh's wave ellipticity curve to assess the three-dimensional seismic response of a sedimentary basin, including the estimation of bedrock depth. Hakim et al. (2019) conducted a study using data from single station measurements to compute the H/V curve and inverted the Rayleigh wave ellipticity curve using DINVER (GEOPSY, 2012), in order to determine the dynamic characteristics of the soil and the distribution of peak surface acceleration on Lombok Island. Issaadi et al. (2020) described a detailed microzonation of Oued-Fodda, in northern Algeria, using the Nakamura method on 102 sites along the city, estimating the soil fundamental frequencies and their corresponding amplitudes. They also estimated the V_s-profiles and provided two cross-sections of the geology beneath the city using the Rayleigh wave ellipticity curve inversion.

This paper shows the results of the numerical inversion of the ellipticity curve alone and with prior knowledge of the average ground properties and borehole data, to assess its reliability to retrieve the shallow structure.

Prior knowledge exists when shear/compression wave velocity of the shallow geological units are reasonably well characterized, as it is common in urban areas, but their thickness may vary laterally.

This paper aims to show that single station measurements can be used as current site investigation technique. It is a low cost and expedite technique that, even with some uncertainty, can give valuable information on the ground shallow structure to support early-stage design decisions, such as:

- estimate bedrock depth, to support the decision on the foundation type (e.g., shallow foundations, underpinning) or the type of technique to be used in the peripherical wall (e.g., soldier pile wall);
- to support the preliminary definition of the ground type, aiming at defining the seismic action (e.g., Eurocode 8).

As the ellipticity curve processing and inversion requires an experienced user, the numerical inversion exploration presented in this paper aims to assess if the ellipticity curve inversion can be done in a routine manner, adopting a straightforward approach to estimate the depth of the impedance contrasts based on simple statistic indicators as the mean or median values of the 30 lower misfit profiles or of all profiles.

This practice oriented paper assesses the uncertainty associated with the inversion of the ellipticity curve to estimate the shallow ground structure, firstly through a numerical simulation of a variety of cases and, secondly, through three normally dispersive case studies in Lisbon County (Portugal). In the case studies, the inversion of the ellipticity curve was done using either the entire or only the right flank of the ellipticity curve.

It is shown that the Rayleigh ellipticity curve can provide valuable, cost-effective information on the depth of a shallow layer overlying a deeper and stiffer layer to support the preliminary design stage in areas where prior knowledge of the ground properties exists.

2. Methodology

The Rayleigh wave ellipticity curve is defined by the ratio between the vertical and horizontal components of the elliptical particle motion due to Rayleigh wave movement as a function of frequency. This ratio is constant in a homogeneous medium, but it is frequency-dependent in a heterogeneous medium due to its dispersive properties (Tokimatsu, 1997).

In the vertical and horizontal components of the recorded seismic wavefield, the contribution of the amplitude of each Rayleigh wave propagation mode, as a function of frequency, is linked to the velocity profile (Malischewsky and Scherbaum, 2004; Wathelet et al., 2008). Therefore, the polarisation or ellipticity curve can be used to estimate the velocity profile. This curve can be calculated through data acquisition with active or passive methods (using a set of stations or a single station) (Foti et al., 2015). Besides the velocity profile, the ellipticity curve depends on the location of the source, the spectrum of the source, the impedance contrast between the soil and the bedrock, and the Poisson's ratio. The relationship between the peak and the trough of the ellipticity curves and their shape, dependent on the impedance contrasts, has been studied by several authors (e.g., Konno and Ohmachi, 1998; Tuan et al., 2011). Nowadays, it is possible to estimate the soil structure by inverting the ellipticity curve (Hobiger et al., 2009).

To obtain the Rayleigh waves' ellipticity curve, Hobiger et al. (2009) developed the RayDec technique for ambient vibrations, based on random decrement technique (Asmussen, 1997), that is usually used to characterise the dynamic properties of buildings, such as resonance frequency and damping, and eliminates all types of waves except Rayleigh's waves. This is done by adding a large number of signal windows with a certain adjustment and calculating the energy of the vertical component and the horizontal components added together to estimate the ellipticity of the Rayleigh wave.

To invert the Rayleigh ellipticity curve, a direct search method called the Neighborhood Algorithm, available in the DINVER tool (GEOPSY, 2012), was used. It was originally proposed by Sambridge (2001) and improved by Wathelet et al. (2004) and Wathelet (2008), the latter version being used in DINVER to invert the ellipticity curve of Rayleigh waves. The Neighborhood Algorithm is a direct search stochastic method and has the advantage of being able to generate new results, considering the previously obtained results (Wathelet, 2008), that is, the method progressively refines the research during the inversion process. It uses Voronoi cells to decompose the parameter space. A misfit value is associated with each cell, and this is calculated for the central point (Wathelet, 2008), with the misfit representing the distance between the experimental curve and the theoretical curve.

The adjustment parameters of the Neighbourhood Algorithm are:

- it_{max}: number of iterations to perform;
- n_{s0}: number of models randomly chosen inside the parameter space at the beginning of the inversion;
- n_s: number of models to generate at each iteration;
- n_r: number of best cells (with the lowest misfit) where the n_s models are generated.

Wathelet (2005) suggested that typical values for n_{s0}, n_r, and n_s are 100, but they may be set to 5, 10 or 50 to force a better optimization. However, with few iterations and a low n_r, the probability of converging to a local minimum is higher.

The total number of models generated (N) in each run corresponds to:

$$N = n_{s0} + it_{max} \cdot n_s \tag{1}$$

If n_s samples are distributed across many cells, a better exploitation of the parameter space will be achieved. In this case, it is recommended to adopt high values of n_r, associated with a high number of iterations. In order to perform a better exploitation, n_s should be higher than n_r.

For a more restricted search, a smaller number of models with a lower misfit should be selected (low n_r). In this work, the adjustment parameters (n_{s0}, it_{max}, n_s) were taken equal to 50, which are DINVER's default value, generating a total of N = 2550 models per run. In this paper, a numerical inversion exploration on the reliability of the V_s-profiles obtained through inversion of the theoretical ellipticity curve for three stiffness contrasts was first performed.

A set of two-layered base models (V_s-profiles) was created considering different V_s contrasts and depth of the seismic impedance contrast.

For each of these base V_s-profiles, the theoretical ellipticity curve was computed using Gpell routine from GEOPSY toolbox. These theoretical ellipticity curves were inverted using DINVER code, taking different input values for shear-wave velocity (V_s) and thickness of the shallow layer (h). For each layer, a V_s search range (SR) were set equal to ±5%, ±20% and ±50% of the V_s-values of the corresponding base V_s-profile to cover different levels of prior knowledge of the site properties. For each combination of input values, the mean and median of all V_s-profiles and of the 30 profiles with the lowest misfit were determined, which were then compared with the base V_s-profile.

To test the reliability of this approach, the methodology was then applied to three normally dispersive case studies in Lisbon with different geological environments. Ambient vibration records were acquired, and data were processed using RayDec to determine the ellipticity curve, which was later inverted using the DINVER code. The mean and median of all V_s-profiles and of the 30 profiles with the lowest misfit were computed and compared with nearby borehole data.

Figure 1 shows a flowchart that summarizes the applied methodology.

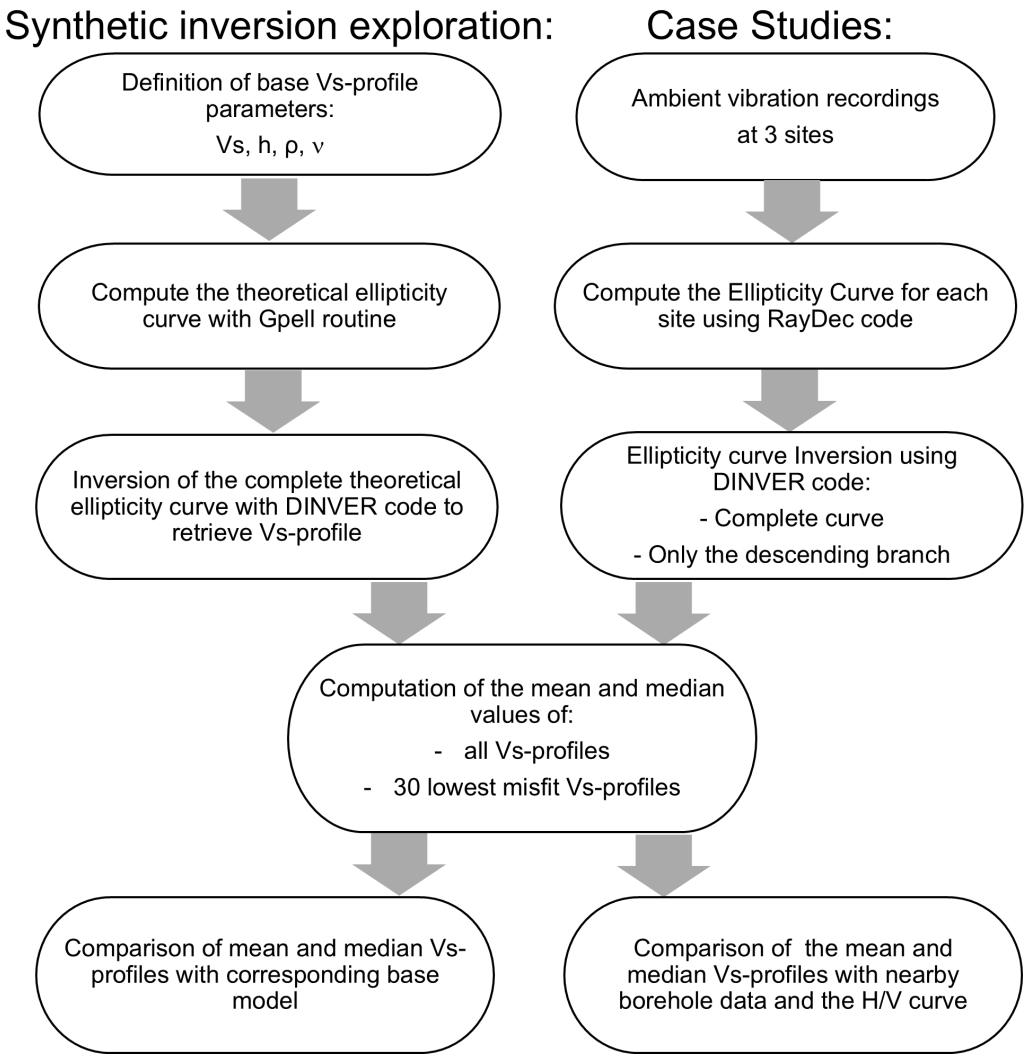

Figure 1. Workflow: numerical inversion exploration and case studies.

3. Numerical inversion exploration

3.1 Introduction

The base V_s-profiles input parameters used to determine the theoretical ellipticity curve using the Gpell subroutine from the GEOPSY software package (GEOPSY, 2012) are summarised in Table 1, where V_s is the S-wave

velocity, ρ the density, and h_B the shallow seismic impedance contrast depth. The Poisson's ratio was held constant in all analyses, and taken equal to 0.4, because the purpose of this numerical inversion exploration is to evaluate the viability and potentiality of this method with minimal amount of information on the ground profile, following the work developed by Hobiger et al. (2013) and Cercato (2017).

Three levels of stiffness contrast (low, medium, and high) and four shallow seismic impedance contrast depth h_B, were analysed, resulting in a total of 12 different base V_s-profiles (Table 1).

Table 1. Properties adopted in the numerical inversion exploration.

Stiffness contrast		ρ (kg/m^3)	V_s (m/s)	h_B (m)
Low ($V_{s,2}/V_{s,1} = 2$)	Layer	1800	200	2, 5, 10, 20
	Half-space	1800	400	
Medium ($V_{s,2}/V_{s,1} = 3$)	Layer	1800	200	
	Half-space	2000	600	
High ($V_{s,2}/V_{s,1} = 5$)	Layer	1800	200	
	Half-space	2000	1000	

The theoretical ellipticity curves computed for each base V_s-profile were then inverted adopting the following input value ranges (see Fig. 2):

- For each layer, V_s search ranges (SR) were set equal to ±5%, ±20% and ±50% of the V_s-values of the corresponding base V_s-profile, assuming different levels of prior knowledge of the site properties (e.g., geological map and generic characteristics of each geological unit).
- ρ – from 1600 to 2400 kg/m^3.
- h_I – free search of the input seismic impedance contrast depth was allowed between 1 m ($h_{I,min}$) and the value defined in Table 2 ($h_{I,max}$) with increments of 1 m, aiming at to test the quality of the solution as a function of the depth ratio DR = $h_{I,max}/h_B$.

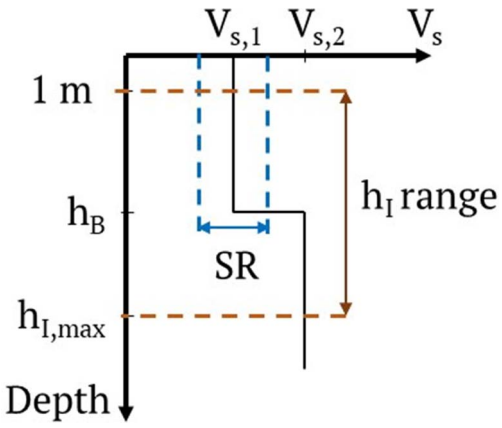

Figure 2. Two-layered base model adopted for the shallow ground structure.

For each h_I value, search range and stiffness contrast, 30 runs were performed, each of them generating 2550 models.

A total of 76500 (= 30 × 2550) models were obtained, 30 of them being minimum misfit models for each h_I.

Considering the high number of simulations and results obtained, the results for the base V_s-profile with h_B = 10 m and an input seismic impedance contrast depth h_I from 1 to 20 m were selected to be shown in detail in the following subsections for the three contrast ratios because they can be taken as representative of all remaining cases.

Table 2. Depth search range adopted in the numerical inversion exploration.

Seismic impedance contrast depth of the base model, h_B (m)	Inversion input contrast depth h_I: from $h_{I,min}$ = 1 m to $h_{I,max}$, with increments of 1 m	Depth ratio range: $DR = h_{I,max}/h_B$
2	from 1 to 4, 10, 20, 30	from 0.5 to 2, 5, 10, 15
10	from 1 to 15, 20, 30	from 0.1 to 1.5, 2, 3
20	from 1 to 25, 30	from 0.05 to 1.25, 1.5

For each contrast case studied, the V_s-profiles obtained using the DINVER code, as well as the corresponding mean and median V_s-profiles, are plotted. The statistical approach (median or average) was applied to all V_s-profile retrieved and to the 30 lowest misfit models, aiming at identifying the best estimate to be applied in practice.

3.2 High, Medium and Low Contrast cases

The V_s-profiles obtained through the inversion of the ellipticity curve associated to the V_s-profile with h_B = 10 m (constraining the seismic impedance contrast depth (h_I) between 1 and 20 m), are presented in Figs. 3, 4-5, showing the influence of the Search Ranges (SR), of adopting the all V_s-profiles or the 30 lowest misfit V_s-profiles, and the mean or median V_s-profiles on the V_s-profile retrieved.

As expected, Fig. 3 shows that the lower misfit V_s-profiles scatter increases with the growth of the search range (SR). However, the mean and median V_s-profiles retrieve with accuracy h (depth of the stiffness contrast), $V_{s,1}$ and $V_{s,2}$ for SR 5% and SR 20%, while for SR 50%, the seismic impedance contrast depth misses by 12 to 22%.

In all cases, $V_{s,1}$ and $V_{s,2}$ are estimated with an error smaller than ~20%.

Figure 4 shows the results for the medium contrast case. The lower misfit V_s-profile scatter increases with the growth of the search range, as in the high contrast case. This scatter, however, is greater than that calculated for the high-contrast case.

For SR 5% and SR 20%, the mean and median V_s-profiles retrieved h (depth of the stiffness contrast), $V_{s,1}$ and $V_{s,2}$ with an error up to 21%, while for SR 50%, the mean and median V_s-profiles retrieved h, $V_{s,1}$ and $V_{s,2}$ with an error up to ~50%.

Finally, for the low contrast case (Fig. 5), it can be seen that the scatter of the lower misfit V_s-profile increases with the growth of the search range, but it is larger than in the previous contrast cases.

For SR 5% and 20%, the mean and median V_s-profiles retrieved $V_{s,1}$ and $V_{s,2}$ with an error up to ~5% and seismic impedance contrast depth with an error up to 4%, while for the 50% search range, the seismic impedance contrast depth errors vary between 9 and 27% and $V_{s,1}$ and $V_{s,2}$ values present errors close to 29%.

Overall, the mean of all V_s-profiles provides the best approach to the base V_s-profile, even if the difference to the other statistical approaches is relatively small.

Observing Figs. 3, 4 and 5, it is possible to see that for the high and medium stiffness contrast cases, the ellipticity curves exhibit a sharp large peak as well as a sharp through. The frequency of the peaks (f_p) varies approximately between 4.0 Hz and 6.0 Hz, for the different search ranges, that is not far from the S-wave resonance frequency of the surface layer (f_0 = 5.0 Hz). These results are in accordance with previous studies on the singularity of H/V Rayleigh waves curves (see, for instance, SESAME, 2004) that showed that the singularity occurs at a frequency that is close to the fundamental resonance frequency for S-waves (f_0) for impedance contrasts larger than 4; for lower impedance contrasts, the ellipticity ratio exhibits a maximum at frequencies that may range between $0.5f_0$ and $1.5f_0$ (Bonnefoy-Claudet et al, 2008). For the lower stiffness contrast the ellipticity curves exhibit also a maximum and a through but less sharp than the previous cases. But it is still possible to identify their frequencies which approximately are 4.0 Hz and 8.0 Hz, respectively. It is interesting to note that Konno and Ohmachi (1998) reported a ratio of two, for the peak and trough frequencies, for a limited set of velocity profiles.

Figure 6 plots the 30 lowest misfit values related to V_s-profiles presented in Figs. 3 to 5.

In all cases, the misfit values grow gently up to the ~30^{th} lowest profiles.

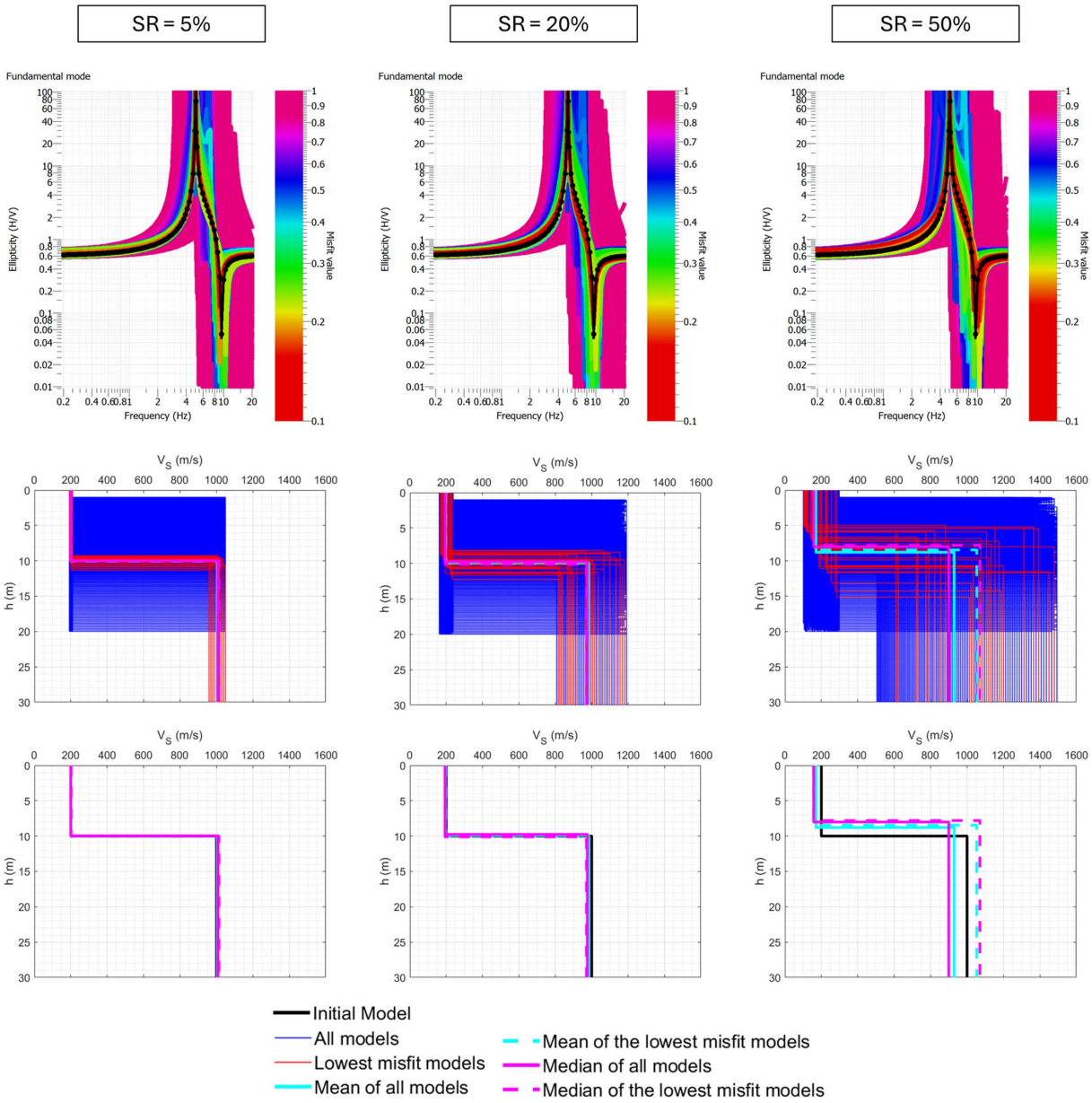

Figure 3. Results retrieved through the inversion of the ellipticity curve associated to the V_s-profile with $V_{s,2}/V_{s,1} = 5$ (high) and stiffness contrast at 10 m depth (h_I) (base model). Inversion performed constraining the position of the stiffness contrast between 1-20 m depth and for different velocity ranges (SR). (a) Ellipticity curves (data points used for the inversion in black), (b) Generated models (c) Mean (blue) and median (red) V_s-profiles, obtained considering: all models (solid line), 30 profiles with lowest misfit (dashed line).

The low contrast case has lower misfit values than the other contrast cases. The medium and the high contrast cases misfit values fall within a relatively narrow range.

The lower misfit values are always associated with the lower SR.

For each stiffness contrast case, the ratio between the 30th lower misfit values and the lowest misfit value are in the range 1.35 to 2.11 for the three contrast cases and SR ranges studied.

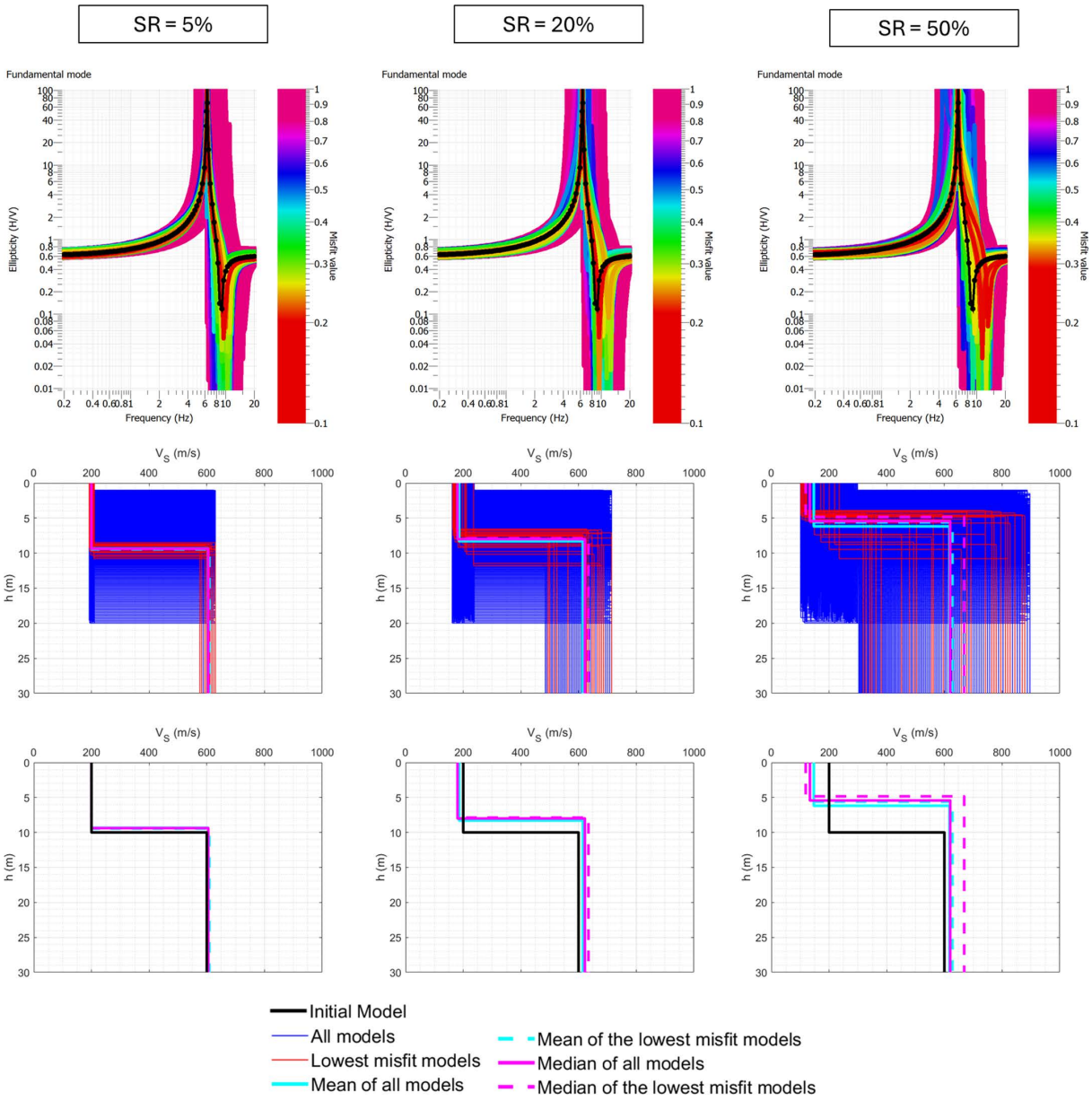

Figure 4. Results retrieved through the inversion of the ellipticity curve associated to the V_s-profile with $V_{s,2}/V_{s,1} = 3$ (medium) and stiffness contrast at 10 m depth (h_I) (base model). Inversion performed constraining the position of the stiffness contrast between 1-20 m depth and for different velocity ranges (SR). (a) Ellipticity curves (data points used for the inversion in black), (b) Generated models (c) Mean (blue) and median (red) V_s-profiles, obtained considering: all models (solid line), 30 profiles with lowest misfit (dashed line).

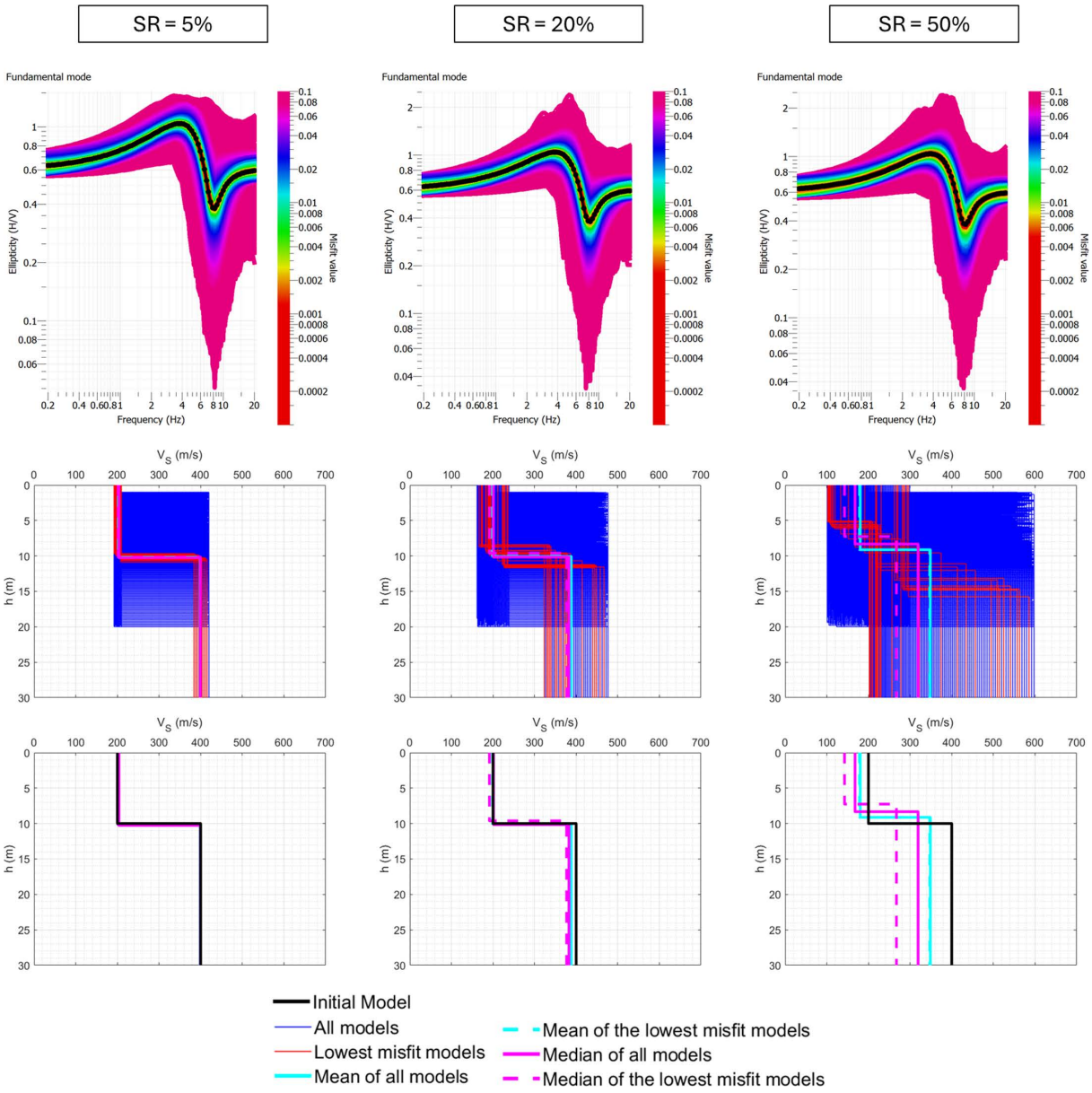

Figure 5. Results retrieved through the inversion of the ellipticity curve associated to the V_s-profile with $V_{s,2}/V_{s,1} = 2$ (low) and stiffness contrast at 10 m depth (h_I) (base model). Inversion performed constraining the position of the stiffness contrast between 1-20 m depth and for different velocity ranges (SR). (a) Ellipticity curves (data points used for the inversion in black), (b) Generated models (c) Mean (blue) and median (red) V_s-profiles, obtained considering: all models (solid line), 30 profiles with lowest misfit (dashed line).

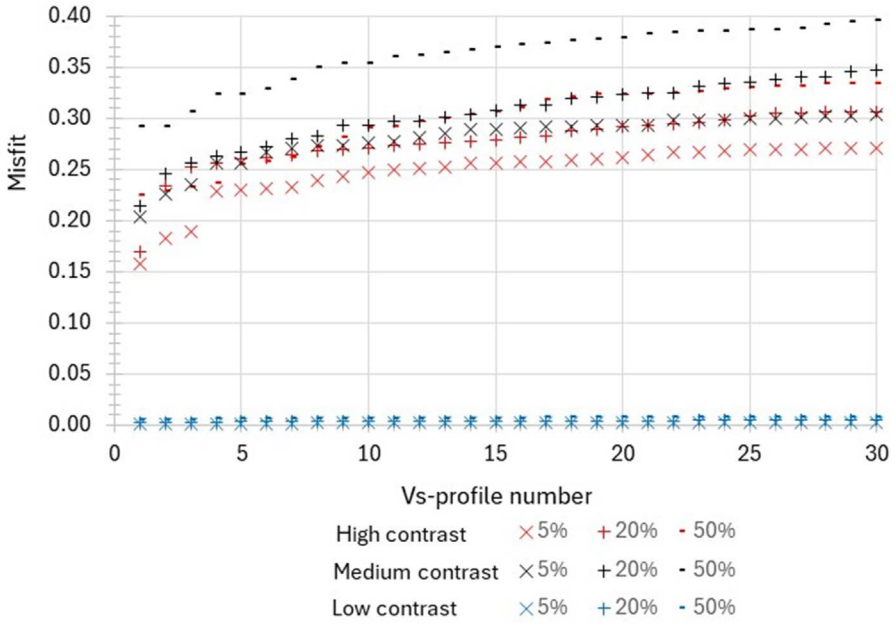

Figure 6. Misfit of the V_s-profiles plotted in Figs. 3 to 5: 30 lowest misfit models.

3.3 Summarized results of all cases

This section summarises the inversion results for all cases investigated, with the goal of determining the impact of the input values used on the retrieved V_s-profiles scatter.

Figure 7 plots the results obtained for the base model with $h_B = 2$ m, which presents a shallower velocity contrast, as a function of the search ranges of the $V_{s,1}$ value and the depth ratio, varying between 1 and $h_{I,max}$, for the three contrast cases studied, namely low, medium and high contrast.

Figure 7 shows that the error to estimate h is less than 10% for SR = 5%, while $V_{s,1}$ and $V_{s,2}$ are retrieved with a very small error. For SR20%, the error to estimate h is smaller than ~15%, while $V_{s,1}$ and $V_{s,2}$ are retrieved with errors up to 16%. For SR50%, the error to estimate h is smaller than ~45%, while $V_{s,1}$ and $V_{s,2}$ are retrieved with errors up to ~40%. These results highlight the importance of having prior knowledge of the ground properties to obtain a model with smaller error.

The mean of all V_s-profiles is, in general, closer to the target point.

For DR higher than 2, the trend is, in general, nearly flat or gently increasing with slight oscillations, thus the DR value in this range has not a relevant impact on the accuracy of the model retrieved. So, DR values larger than 2 are recommended to increase the exploited range.

Figure 8 plots the results obtained for the base model with shallow seismic impedance contrast depth, h_B, equal to 10 and 20 m, which presents the deepest velocity contrast studied in this work, as a function of the search ranges of the $V_{s,1}$ value and the depth ratio, varying between 1 and $h_{I,max}$, for the three contrast cases studied, namely low, medium and high contrast. In this figure, the statistical approach (median or average) to estimate the V_s-profile are based on all models.

Figure 8 shows that:

- A search range equal to 5% or even 20%, results in a good fit with the base V_s-profile, whereas a search range equal to 50% results in a large scatter, demonstrating the importance of prior knowledge of V_s-values.
- Overall, for both depths (10 and 20 m), there is a slight convergence of the data to the base V_s-profile better for the mean of all V_s-profiles than for the median.

Analyzing the results, it can be seen that the dots more distant from the target are associated to low DR values. For DR > 2, a closer fit of h, $V_{s,2}$ and $V_{s,1}$ is obtained.

Figure 9 plots the results obtained for the base model with shallow seismic impedance contrast depth, h_B, equal to 10 and 20 m, which presents the deepest velocity contrast studied in this work, as a function of the search ranges

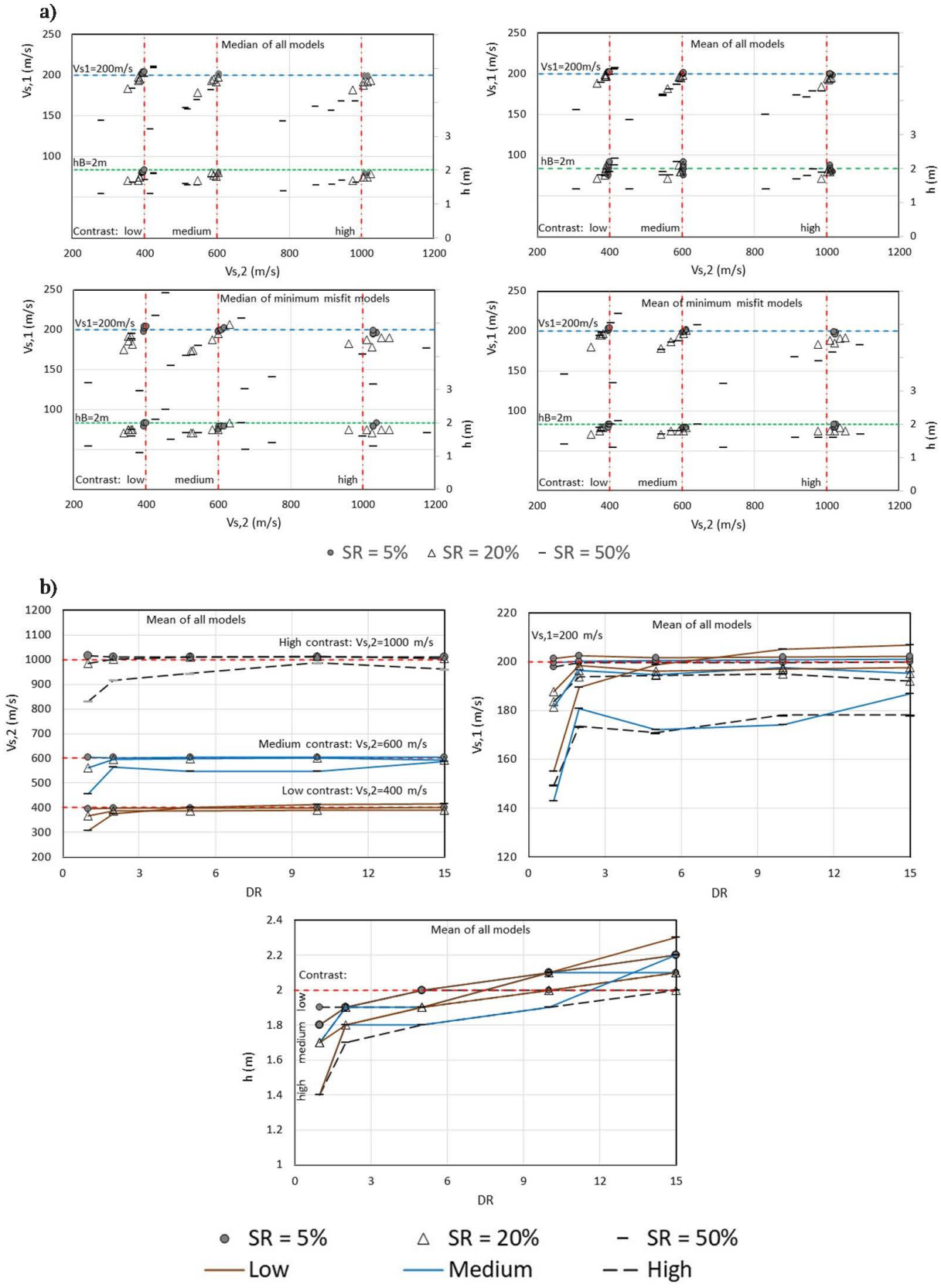

Figure 7. Base V_s-profile with shallow seismic impedance contrast depth $h_B = 2$ m: (a) effect of the search range (SR), stiffness contrast and statistical approach (median or average); (b) effect of depth ratio $DR = h_{I,max}/h_B$ (mean of all models).

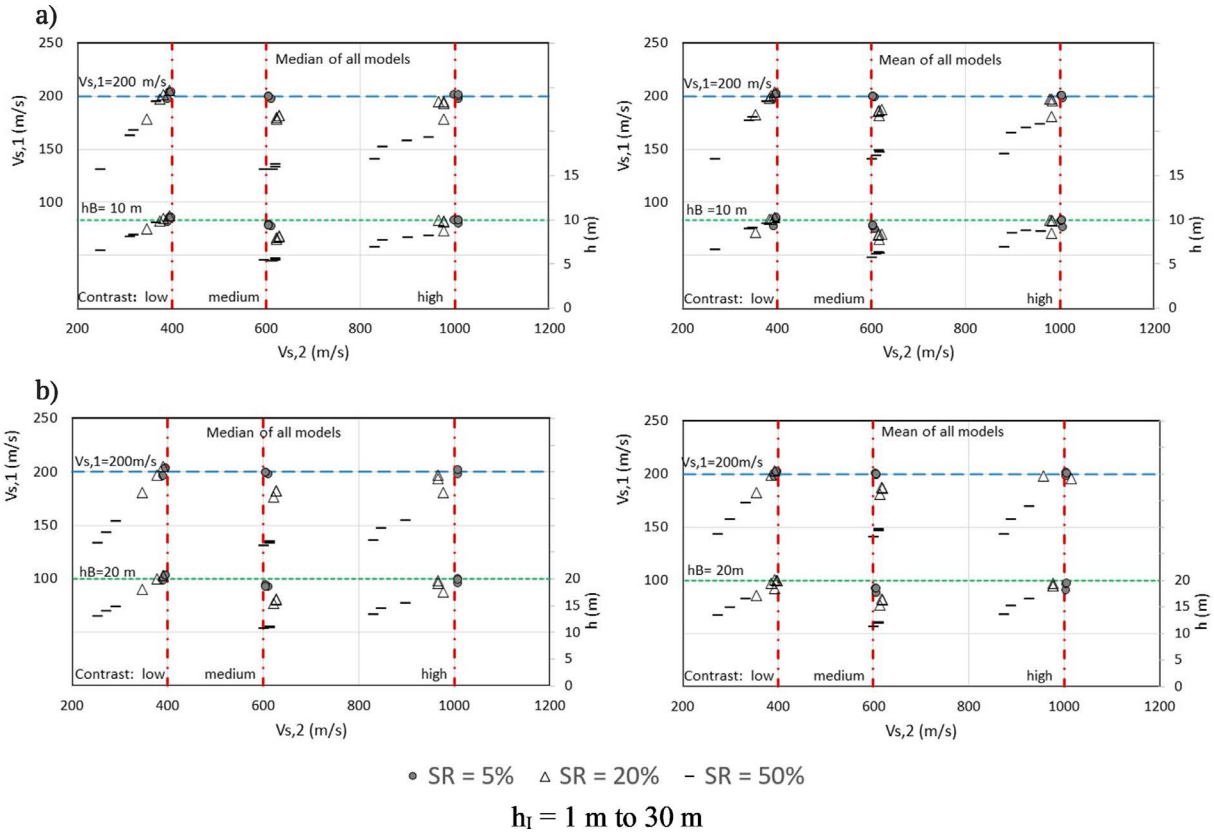

Figure 8. Base models with shallow seismic impedance contrast depth at: (a) h_B = 10 m; (b) h_B = 20 m: effect of contrast ratio (low, medium and high), search range (SR) for parameter $V_{s,1}$ and statistical approach (median or average) to estimate the V_s-profile based on all models.

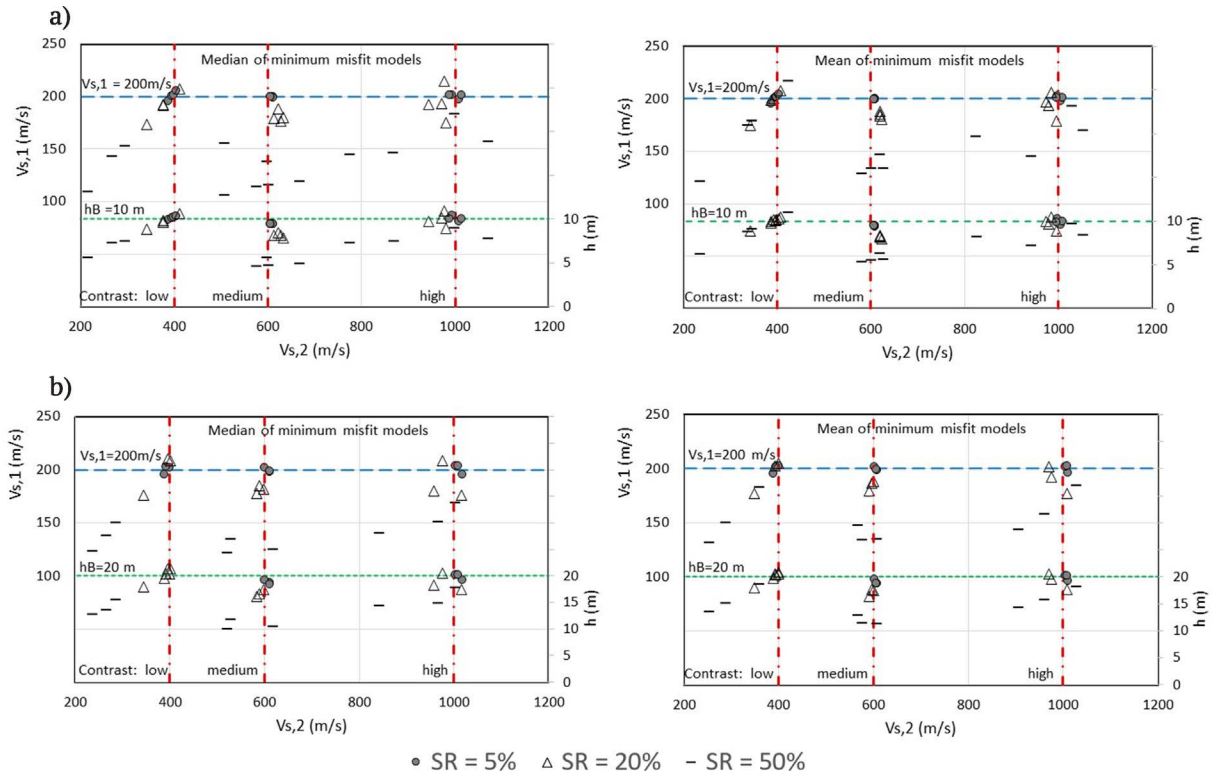

Figure 9. Base models with shallow seismic impedance contrast depth at: (a) h_B = 10 m; (b) h_B = 20 m: effect of contrast ratio (low, medium and high), search range (SR) for parameter $V_{s,1}$ and statistical approach (median or average) to estimate the V_s-profile based on 30 minimum misfit models.

of the $V_{s,1}$ value and the depth ratio, varying between 1 and $h_{I,max}$, for the three contrast cases studied, namely low, medium and high contrast. In this fig., the statistical approach (median or average) to estimate the V_s-profile are based on 30 minimum misfit models.

The trend observed in Fig. 9 is similar to the one observed in Fig. 8.

Globally, the mean of the lowest misfit V_s-profiles provides a closer match to the base V_s-profile than the median of the lowest misfit V_s-profiles and it is in the same range as the mean of all V_s-profiles.

Based on Figs. 7, 8-9, it can be seen that the means of the V_s-profiles (all or the 30 with the lowest misfit) better match the base V_s-profile than the corresponding median values.

The results scatter show that it is important to have an estimation of the V_s-values with an error less than 20% to retrieve a ground profile model close to the real soil structure. And the search range for the seismic impedance contrast depth should be wide to obtain better fits.

4. Case-studies

4.1 Introduction

Three case studies are presented to demonstrate the ellipticity curve's potential as a cost-effective preliminary site investigation technique when prior knowledge exists.

Ambient vibrations were recorded at three different locations in Lisbon County, with the following geological settings characterized by borehole data (Fig. 10):

- Campolide site, at Rua de Campolide: A 13-meter far geotechnical borehole reveals a landfill layer reaching 15.8 m over a rock geological formation known as the Lisbon Volcanic Complex (LVC).
- Chelas site, Bairro do Condado, Rua J A2: the nearby geotechnical borehole shows 5 m thick cover landfills laying over Chelas Valley Sands (CVS).
- Parque das Nações site, at Caminho da Rainha: a 2 m far geotechnical borehole shows 10 m thick cover landfills, over 12.3 m of alluvium, lying over Marvila Limestones (ML).

The ambient vibration acquisitions were recorded for ~30 min at each site, using a Cityshark digitiser coupled with a 3D Lennartz Lite seismometer of 1 s period, with a sampling rate of 100 ms. The data was detrended, baseline corrected and 200 Hz low-pass filtered in order to avoid aliasing.

The measurements were taken in favorable weather conditions (no rain and no wind or light breeze), and the sensor was installed directly on soil or asphalt.

For each ambient vibration measurement, the H/V curve was computed using Geopsy software (GEOPSY, 2012), and the peak frequency (f_0 and f_1, when available) and corresponding amplitude were identified. SESAME guidelines (SESAME, 2004) were used to evaluate the reliability of the H/V curves that were calculated.

The buffered signal windows to determine the ellipticity curve was taken equal to 10/f, to have at least ten cycles for a good coverage, as recommended by Hobiger et al. (2009).

The RayDec technique (Hobiger et al., 2009) was used to compute the mean experimental Rayleigh wave ellipticity curve. The ellipticity curve was inverted using DINVER code to retrieve the V_s-profile, either using the complete curve or just the right flank, because the right flank of the ellipticity peak and peak frequency carry the important information of the soil structure (e.g., Hobiger, 2011). The density was taken between 1600 kg/m^3 and 2400 kg/m^3, and the Poisson's ratio value was taken equal to 0.4.

DINVER generated 76500 V_s-profiles for each simulation. The median and mean of all V_s-profiles, as well as the median and mean of the 30 V_s-profiles with lowest misfit were computed and compared to nearby borehole data. In addition, each median and mean V_s-profile obtained was used to compute the corresponding theoretical ellipticity curves, which were compared with the mean experimental ellipticity curve and the H/V curve calculated from the recordings.

4.2 Results and discussion

The ambient vibration recordings acquired at the 3 normally dispersive sites were processed, and the results are presented in Fig. 10, as well as a schematic borehole profile.

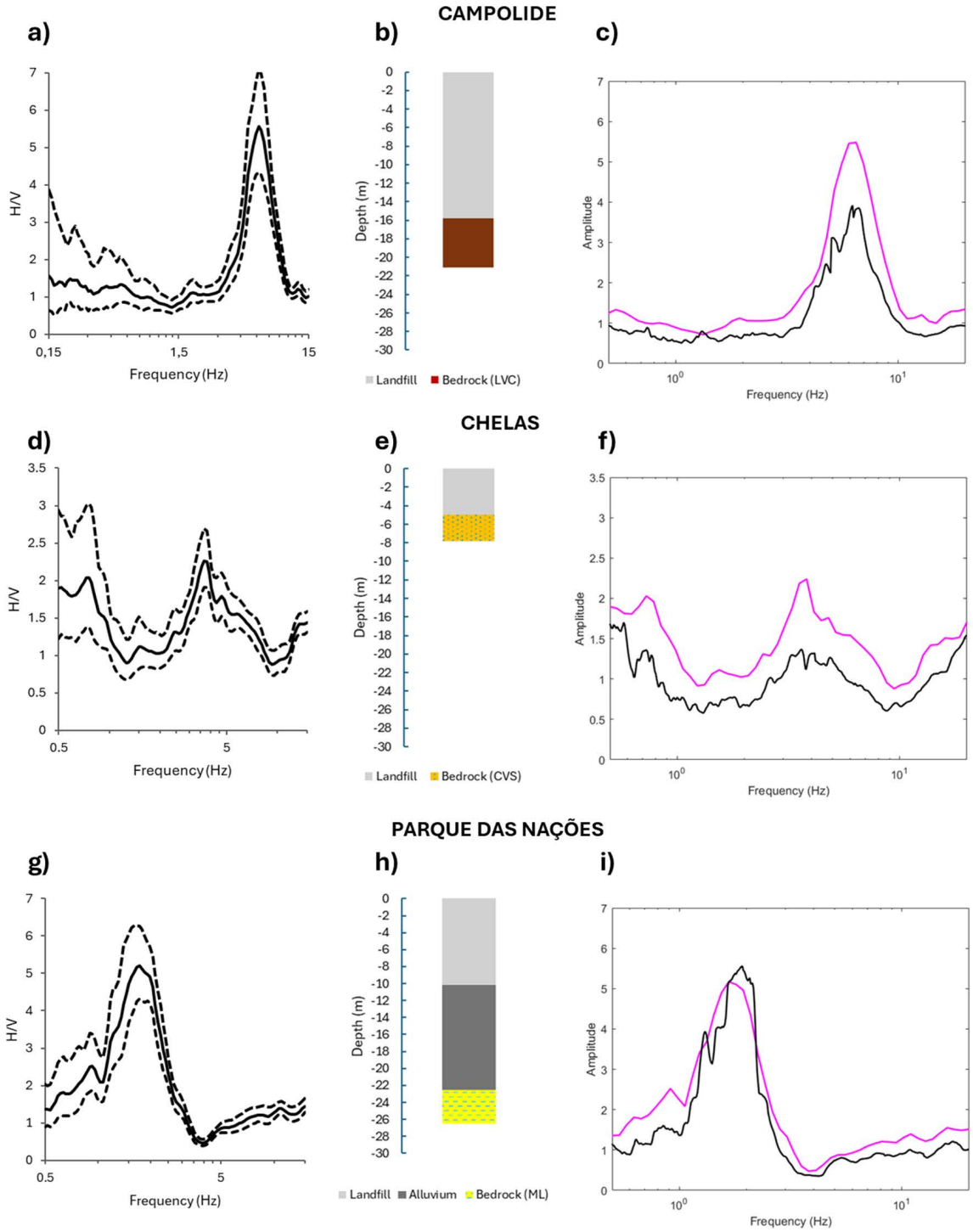

Figure 10. Case studies sites: (a, d, g) H/V curves (black line-average curve; dashed black lines-average plus and minus one standard deviation) (b, e, h) borehole soil profile; (c, f, i) ellipticity curves (black line–average curve) and average H/V curve (pink line).

For the three cases, the ellipticity (black line) and H/V (pink line) average curves have similar shape but, with the exception of Parque das Nações site, the ellipticity curve has lower ordinates (Figs. 10c-f-i). Because the H/V curve contains the contribution of all seismic waves, while the ellipticity curve depends only on the Rayleigh waves, the wave field in Parque das Nações site is dominated by Rayleigh waves, while in the other two sites body and Love waves must have a relevant contribution to the wave field.

The Campolide H/V curves exhibits a very well-defined peak at ~6.3 Hz with an amplitude of ~5, an evidence of an high impedance contrast, whereas the Chelas H/V curves have a smaller amplitude (~2) but also a well-defined

peak at ~3.9 Hz, evidencing a lower impedance contrast. The H/V curves in Parque das Nações similarly exhibit a well-defined peak at ~1.66 Hz, with an amplitude of ~5 (Fig. 10a, d and g), evidencing an high impedance contrast. These peaks correspond to the impedance contrast between the cover layers (landfill or landfill + alluvium) and the base formations (Fig. 10b, e and h).

Table 3 shows the V_s search range used for the inversion of the recorded experimental ellipticity curves for the three case studies, based on V_s measurements taken in these layers but in diverse parts of the city. The stratification of the profiles was determined using the closest geotechnical borehole data (see Fig. 10b, e and h).

Table 3. Initial parameters adopted for the two-layers inversion (ν = 0.4) for the three case studies.

Site	Statigraphy	Search range V_s (m/s)	h_I (m)
Campolide	Landfill Bedrock (LVC)	175 – 400 (SR = ~33%) 800 – 2000 (SR = ~50%)	1 to 20 –
Chelas	Landfill Bedrock (CVS)	100 – 150 (SR = ~20%) 200 – 400 (SR = ~33%)	1 to 10 –
Parque das Nações	Landfill + Alluvium Bedrock (ML)	100 – 200 (SR = ~33%) 500 – 2000 (~60%)	1 to 30 –

Figure 11 depicts the results of inverting the whole ellipticity curve and only the right flank, because the complete ellipticity curve may not be retrieved from the ambient vibration measurements, and the paper's goal is to propose a methodology that is straightforward to apply with minimal prior knowledge to decide the relevant flank of the ellipticity curve to be used in the inversion.

In general, the fit between the theoretical and the mean experimental ellipticity curves for Campolide is reasonable, either using the whole curve or only the right flank (Figs. 11b-d). The complete theoretical ellipticity curve in Chelas (Fig. 11f), has a satisfactory fit to the mean experimental ellipticity curve, and the right flank of the theoretical ellipticity curve (Fig. 11h) has a very good fit to the mean experimental ellipticity curve. The theoretical ellipticity curve for Parque das Nações displays a fair fit to the mean experimental ellipticity curve, whether utilizing the whole curve or only the right flank (Figs. 11j-l, respectively). However, the data points adjustments present some imperfections in particular for the inversion of the right flank in Campolide and Parque das Nações sites. This can be due to the heterogeneity of the surficial layer because the measurements were not carried out directly on soil but on an asphalt surface.

The results plotted in Fig. 11 show high stiffness contrast and relatively deep for Campolide (1100/230 = ~4.8 about 9 to 15 m deep) and Parque das Nações (730/240 = ~3.0 about 21.5 and 28 m deep) (see Fig. 11), while for Chelas the stiffness contrast is moderate and shallow (280/130 = ~2.2 between 4.5 and 7 m deep).

Table 4. The consistency between the resonance frequency peaks observed in H/V and Rayleigh wave ellipticity curves, obtained from the inversion of the complete curve, and the 1D subsurface models retrieved.

Site	V_s shallow layer (m/s)	Stiffness contrast	Depth of the shallower seismic impedance contrast, H (m)	$f_o = V_s/(4H)$ (Hz)	f_o,H/V (Hz)	Amplitude H/V curve
Campolide	230	~4.8	Mean all: 9 Mean 30 lowest: 15	6.4 3.8	6.3	~5
Chelas	130	~2.2	Mean all: 4.5 Mean 30 lowest: 7	7.2 4.6	3.9	~2
Parque das Nações	240	~3.0	Mean all: 21.5 Mean 30 lowest: 28	2.8 2.1	1.7	~5

Table 4 compares the resonance frequency peaks observed in H/V and Rayleigh ellipticity curves (inversion of the complete curve) and the 1D subsurface models retrieved. The value of f_o was computed with the V_s value of the shallow layer.

The H/V peak frequency is close to the peak frequency associated with the shallower contrast and estimated through the equation $V_s/4H$. For Campolide the frequency fit is better for the depth estimated with the mean of all models, while for Chelas and Parque das Nações the best fit is for the mean of the 30 lowest misfit models.

Also, it can be noticed an higher stiffness contrast when the amplitude of the H/V peak is higher.

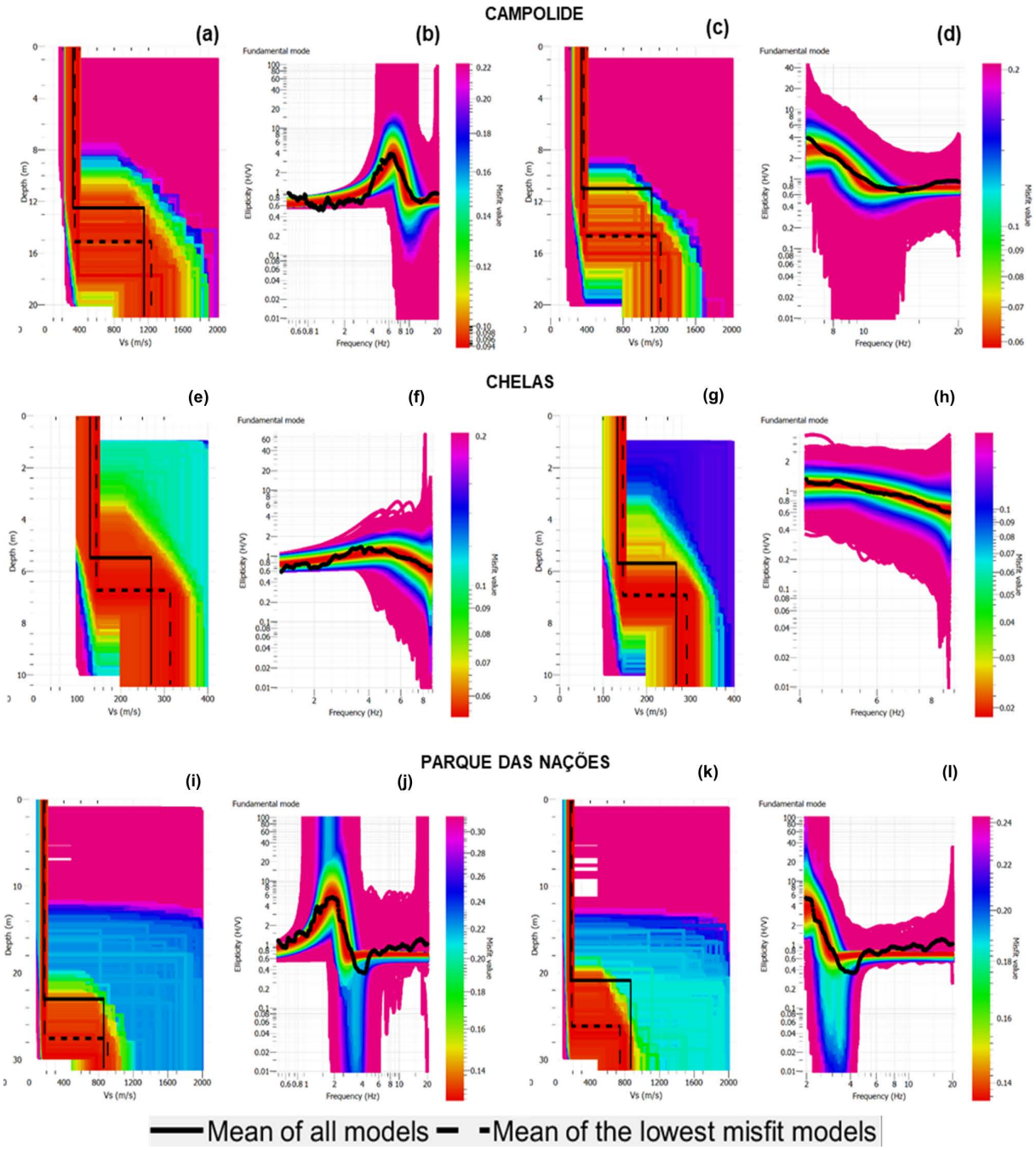

Figure 11. Vs-profiles retrieved for the three case studies: (a, e, i) complete ellipticity curve inversion; black lines show the mean Vs-profiles; (b, f, j) mean experimental ellipticity curve (in black) and theoretical ellipticity curves computed with the DINVER program, after complete curve inversion; (c, g, k) right flank inversion; black lines show the mean Vs-profiles; (d, h, l) mean experimental ellipticity curve (in black) and theoretical ellipticity curves computed with the DINVER program, after right flank inversion.

The method provided a good fit between measured and estimated frequencies for the case-studies with higher stiffness contrast.

Figure 12 depicts graphs for the ground profiles of all case studies, considering:

- The mean of all V_s-profiles produced by inverting the whole ellipticity curve (Ellipticitycompl/mean all) and the right flank only (EllipticityRight/mean all).
- The mean of the 30 lowest misfit V_s-profiles derived from inverting the whole ellipticity curve (Ellipticitycompl/mean 30low) and the right flank only (EllipticityRight/mean30 low).
- Average V_s measured in each geologic formation in Lisbon County at similar depth range (Oliveira et al., 2023).
- V_s-profile obtained from a linear array active seismic acquisition performed by Oliveira et al. (2021) (using MASW).

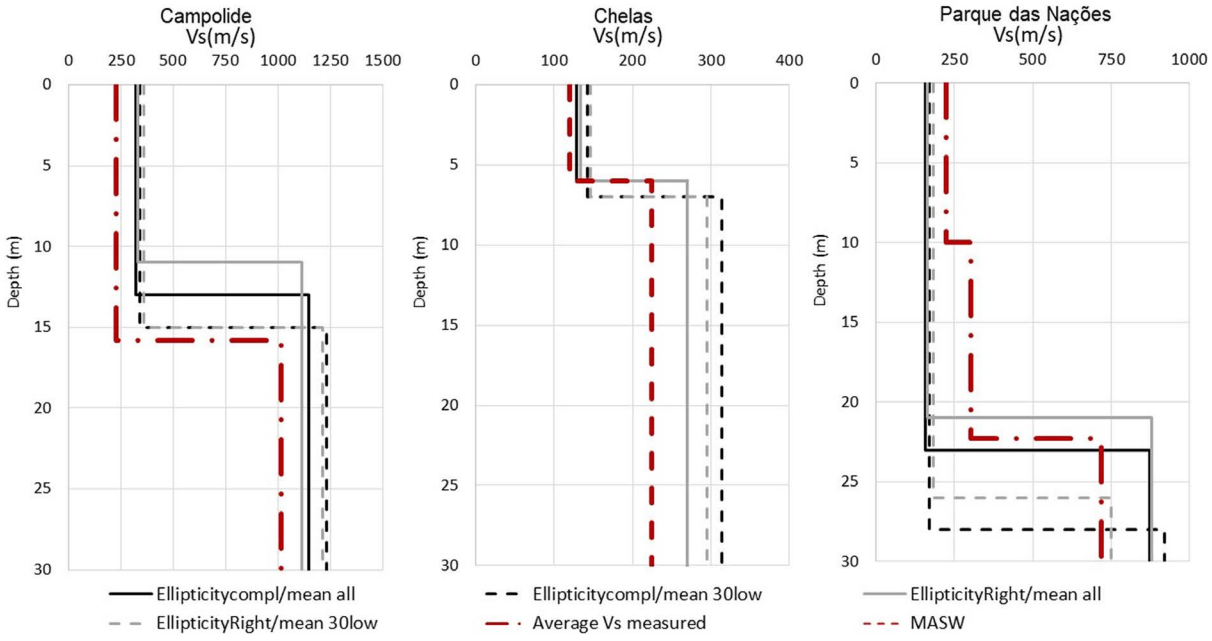

Figure 12. Comparison between the V_s-profiles retrieved form ellipticity curve inversion with borehole data/MASW.

From the analysis of Fig. 12 in can be seen that:

- Globally, the V_s-profiles from the inversion are in good agreement with the V_s-profiles based in V_s measurements and borehole data.
- The V_s-profiles produced from the Rayleigh wave ellipticity analysis retrieve the seismic impedance contrast depth fairly well, generally with an error margin not exceeding 20%. No combination is shown to adapt better than the others.
- The V_s-values retrieved from the Rayleigh wave ellipticity analysis are lower or higher than the V_s measured profile, within an error margin not more than 30%, in general, being lower for $V_{s,1}$ than for $V_{s,2}$.

5. Conclusions

The inversion of single-station Rayleigh wave ellipticity curve in routine site investigation can be an interesting tool.

This research includes a numerical inversion exploration as well as three normally dispersive case studies that show how the Rayleigh wave ellipticity curve yields cost-effective information on the shallow ground structure useful for limited spaces in urban areas.

The numerical study assumed a top layer with $V_s = 200$ m/s, overlaying a stiffer layer with $V_s = 400$, 600 or 1000 m/s, and the interface between layers varied between 2, 5, 10 and 20 m. The three case-studies had top layer V_s between ~130 and ~280 m/s, overlaying a layer with V_s = ~200 to 1000 m/s, and interface depth between 5 to 25 m, based on borehole data and surface seismic measurements.

The search range of the V_s value varied between 5%, 20% and 50% in the numerical study, while in the case studies varied between 20 to 60% of the expected V_s value.

The numerical inversion exploitation shows that: (i) globally, the mean of the lowest misfit V_s-profiles provides a closer match to the base V_s-profile than the median of the lowest misfit V_s-profiles and it is in the same range as the mean of all V_s-profiles. (ii) The results scatter show that it is important to have an estimation of the V_s-values with an error less than 20%, to retrieve a ground profile model close to the real soil structure.

The search range for the seismic impedance contrast depth should at least 2 time larger than the real seismic impedance contrast depth to obtain better fits.

Three normally dispersive case studies in Lisbon County demonstrated the potential of using the ellipticity curve computed from ambient vibration measurements. The ellipticity curve inversion provides V_s-profiles that closely fit the estimated V_s-profile. Furthermore, there is good agreement between the theoretical ellipticity curves estimated for the means of the V_s-profiles and the mean experimental ellipticity curve. For the depths and stiffness contrasts covered by the case studies, reliable results can be obtained with the inversion of the right flank.

The use of the Rayleigh wave ellipticity curve is demonstrated to be a beneficial and cost-effective site investigation technique to assess the shallow ground structure model when prior knowledge of the ground properties exists, as it is common in urban areas.

The trends detected need to be confirmed in other geological environments, such as covering a wither range of impedance contrast and inversely dispersive profiles, to extend the conclusion of this paper.

Data availability statement. Share upon reasonable request data sharing policy.

Acknowledgements. The authors would like to thank the support of the Municipality of Lisbon (CML), which provided access to the geotechnical database of Lisbon. The author Rui Carrilho Gomes would like to thank the financial support of the Foundation for Science and Technology, through the project UIDB/04625/2025 of the CERIS research unit.

References

Arai, H. and K. Tokimatsu (2005). S-wave velocity profiling by joint inversion of microtremor dispersion curve and horizontal-to-vertical (H/V) spectrum, Bull. Seismol. Soc. Am., 95, 5, 1766-1778, doi:10.1785/0120040243.

Asmussen, J. C. (1997). Modal Analysis Based on the Random Decrement Technique: Application to civil engineering structures, PhD Thes, Dept. Build. Technol. Struct. Eng., 227.

Bonnefoy-Claudet, S., A. Kohler, C. Cornou, M. Wathelet et al. (2008). Effects of Love Waves on Microtremor H/V Ratio, Bull. Seismol. Soc. Am., 98, 1, 288-300, doi:10.1785/0120070063.

Corchete, V. (2013). A methodology for the analysis of the Rayleigh-wave ellipticity, Earth Sci. Res. J., 17, 2, 127-133.

Di Giulio, G., M. Ercoli, M. Vassallo and M. Porreca (2020). Investigation of the Norcia basin (Central Italy) through ambient vibration measurements and geological surveys, Eng. Geol., 267, 105501, doi:10.1016/j.enggeo.2020.105501.

Fäh, D., F. Kind and D. Giardini (2003). Inversion of local S-wave velocity structures from average H/V ratios, and their use for the estimation of site-effects, J. Seismol., 7, 4, 449-467.

Foti, S., C. Lai, G. Rix and C. Strobbia (2014). Surface Wave Methods for Near-Surface Site Characterization, CRC Press, London, 487, doi:10.1201/b17268, ISBN:9780429178535.

Geopsy (2012). Geopsy: Software applications for ambient vibration techniques Geopsy project, Available, http://www.geopsy.org/.

Gouveia, F., I. Lopes and R. C. Gomes (2016). Deeper Vs profile from joint analysis of Rayleigh wave data, Eng. Geol., 202, 85-98, doi:10.1016/j.enggeo.2016.01.006.

Hakim, A. C., S. Pramono, D. D. Warnana, J. P. G. N. Rochman et al. (2019). Determination of Ground Profile and Peak Surface Acceleration (PSA) using single station microtremor Inversion method for earthquake hazard zonation of Lombok Island, in Geomatics International Conference, IOP Publishing, Surabaya, Indonesia, 389, 1, 012045, doi:10.1088/1755-1315/389/1/012045, ISSN:1755-1307.

Hobiger, M. (2011). Polarisation des ondes de surface: Caractérisation, inversion et application à l'étude de l'aléa sismique, PhD Thesis, University of Grenoble, Grenoble, France, 250.

Hobiger, M., P. Y. Bard, C. Cornou and N. Le Bihan (2009). Single station determination of rayleigh wave ellipticity by using the random decrement technique (RayDec), Geophys. Res. Lett. 36, 14, L14303, doi:10.1029/2009GL038863

Hobiger, M., C. Cornou, M. Wathelet, G. D. Giulio et al. (2013). Ground structure imaging by inversions of Rayleigh wave ellipticity: sensitivity analysis and application to European strong-motion sites, Geophys. J. Int., 192, 1, 207-229, doi:10.1093/gji/ggs005.

Issaadi, A., F. Semmane, A. Yelles-Chaouche, J. J. Galiana-Merino et al. (2020). A shear-wave velocity model in the city of oued-fodda (Northern Algeria) from Rayleigh wave ellipticity inversion. Appl. Sci., 10, 5, 1717, doi:10.3390/app10051717.

Konno, K. and T. Ohmachi (1998). Ground-Motion Characteristics Estimated from Spectral Ratio between Horizontal and Vertical Components of Microtremor, Bull. Seismol. Soci. Am., 88, 1, 228-41, doi:10.1785/BSSA0880010228.

Leyton, F., S. Ruiz, S. A. Sepúlveda, J. P. Contreras et al. (2013). Microtremors' HVSR and its correlation with surface geology and damage observed after the 2010 Maule earthquake (Mw 8.8) at Talca and Curicó, Central Chile, Eng. Geol., 161, 26-33, doi:10.1016/j.enggeo.2013.04.009.

Lunedei, E. and P. Malischewsky (2015). A Review and Some New Issues on the Theory of the H/V Technique for Ambient Vibrations, Ansal, A. (eds), Perspectives on European Earthquake Engineering and Seismology, Geotechnical, Geological and Earthquake Engineering, Springer, Dordrecht, 39, 15, 371-394, ISSN 1573-6059.

Malischewsky, P. and F. Scherbaum (2004). Love's Formula and H/V-Ratio (Ellipticity) of Rayleigh Waves, Wave Motion, 40, 1, 57-67, doi:10.1016/j.wavemoti.2003.12.015.

Maranò, S., M. Hobiger and D. Fäh (2017). Retrieval of Rayleigh wave ellipticity from ambient vibration recordings, Geophys. J. Int., 209, 21, 334-352, doi:10.1093/gji/ggx014.

Molnar, S., J. Assaf, A. Sirohey and S. R. Adhikari (2020). Overview of local site effects and seismic microzonation mapping in Metropolitan Vancouver, British Columbia, Canada, Eng. Geol. 270, 105568, doi:10.1016/j.enggeo.2020.105568.

Maklad, M., T. Yokoi, T. Hayashida, M. N. ElGabry et al. (2020). Site characterization in Ismailia, Egypt using seismic ambient vibration array, Eng. Geol., 279, 105874, doi:10.1016/j.enggeo.2020.105874.

Nakamura, Y. (1989). A Method for Dynamic Characteristics Estimation of Subsurface Using Microtremor on the Ground Surface, Quarterly Report, Railway Technical Research Institute/Tetsudo Gijutsu Kenkyujo, Tokyo, 30, 25-33, ISSN: 0033-9008.

Oliveira, L., P. Teves-Costa, C. Pinto, R. C. Gomes et al. (2020). Seismic microzonation based on large geotechnical database: Application to Lisbon, Eng. Geol., 265, 105417, doi:10.1016/j.enggeo.2019.105417.

Oliveira, L., P. Teves-Costa, R. C. Gomes, I. M. Almeida et al. (2021). Lisbon seismic microzonation based on penetration tests and surface seismic methods, XVII Congresso Nacional de Geotecnia, Lisboa, www.researchgate.net/publication/362093429.

Oliveira, L., R. C. Gomes and P. Teves-Costa (2023). Contribution to the seismic microzonation of Lisbon based on the integration of geological, geophysical, and geotechnical data, Soil Dyn. Earthq. Eng., 171, 107965, doi:10.1016/j.soildyn.2023.107965.

Pastén, C., M. Sáez, S. Ruiz, F. Leyton et al. (2016). Deep characterization of the Santiago Basin using HVSR and cross-correlation of ambient seismic noise, Eng. Geol., 201, 57-66, doi:10.1016/j.enggeo.2015.12.021.

Poggi, V., D. Fäh, J. Burjanek and D. Giardini (2012). The use of Rayleigh-wave ellipticity for site-specific hazard assessment and microzonation: application to the city of Lucerne, Switzerland, Geophys. J. Int., 188, 3, 1154-1172, doi:10.1111/j.1365-246X.2011.05305.x.

Sambridge, M. (2001). Finding acceptable models in nonlinear inverse problems using a neighbourhood algorithm, Inverse Probl., 17, 387-403, doi:10.1088/0266-5611/17/3/302.

Tokimatsu, K. (1997). Geotechnical Site Characterization Using Surface Waves. Proceedings of the 1st International Conference on Earthquake Geotechnical Engineering, Japanese Society of Soil Mechanics and Foundation Engineering (Editor), International Society for Soil Mechanics and Foundation Engineering, Rotterdam, 1333-1368, ISBN: 905410578X.

Tuan, T. T., F. Scherbaum and P. G. Malischewsky (2011). On the Relationship of Peaks and Troughs of the Ellipticity (H/V) of Rayleigh Waves and the Transmission Response of Single Layer over Half-Space Models, Geophys. J. Int., 184, 3, 793-800, doi:10.1111/j.1365-246X.2010.04863.x.

Wathelet, M., D. Jongmans and M. Ohrnberger, (2004). Surface-wave inversion using a direct search algorithm and its application to ambient vibration measurements, Near Surf. Geophys., 2, 4, 211-221, doi:10.3997/1873-0604.2004018.

Wathelet, M. (2005). Array Recordings of Ambient Vibrations: Surface-Wave Inversion, PhD Thesis, University of Liège, Liège, Belgium.

Wathelet, M. (2008). An improved neighborhood algorithm: parameter conditions and dynamic scaling, Geophys. Res. Lett., 35, L09301, doi:10.1029/2008GL033256.

Yilar, E., L. G. Baise and J. E. Ebel, (2017). Using H/V measurements to determine depth to bedrock and Vs30 in Boston, Massachusetts, Eng. Geol., 217, 12-22, doi:10.1016/j.enggeo.2016.12.002.

SESAME Team, 2004. Guidelines for the implementation of the H/V spectral ratio technique on ambient vibrations – measurements, processing and Interpretation, SESAME European Research Project, WP12-Deliverable D23.12, European Commission – Research General Directorate, Project No. EVG1-CT-2000-00026, 1-62.

***CORRESPONDING AUTHOR: Rui Carrilho GOMES**,
Instituto Superior Técnico, Universidade de Lisboa, Lisbon, Portugal
e-mail: rui.carrilho.gomes@tecnico.ulisboa.pt